Modeling and Velocity Control for a Novel Narrow Vehicle Based on Mobile Wheeled Inverted Pendulum

Jian Huang, *Member, IEEE*, Feng Ding, Toshio Fukuda, *Fellow, IEEE*, and Takayuki Matsuno

***Abstract*— Traffic problems such as pollution and congestion are becoming more and more serious in urban areas. A potential solution to these problems is to develop narrow vehicles that occupy less space and have lower emissions. There has been increasing interest in underactuated mechanical systems, i.e., mobile wheeled inverted pendulum (MWIP) models, which are widely used in the field of autonomous robotics and intelligent narrow vehicles. A novel narrow vehicle based on an MWIP and a movable seat, called UW-Car, is investigated in this paper. The dynamic model of the underactuated vehicle system running on flat ground is derived by Lagrange's equation of motion. Based on the dynamic model and terminal sliding mode control method, two terminal sliding mode controllers are designed to control velocity and braking of the UW-Car. The first one is used to control the forward speed to a desired value while keeping the body upright and the seat on some fixed position. The second one is a switching sliding mode controller, composed of three terminal sliding mode controllers that quickly brakes the system according to an optimal braking scheme. All the control algorithms are tested in both MATLAB simulation and a UW-Car experiment. The simulation and experimental results demonstrate the efficiency of the model and controllers.**

***Index Terms*— Dynamic modeling, mobile wheeled inverted pendulum (MWIP), optimal braking, terminal sliding mode control, velocity control.**

I. INTRODUCTION

PARKING, pollution, and congestion problems caused by vehicles in urban areas have made life uncomfortable and inconvenient. To improve living conditions, developing an intelligent, self-balanced, and less polluting narrow vehicle might be a good idea. In pursuance of this idea, many autonomous robots and intelligent vehicles have been implemented based on mobile wheeled inverted pendulum (MWIP) models [1]–[7] such as PMP [1], nBot [2], and Segway [3].

The MWIP models have attracted much attention in the field of control theory because they are nonlinear and underactuated with inherent unstable dynamics. Many previous works used linear [8], [9] or feedback linearization methods [10]–[13] in their modeling and control. They rely on a rather precise description of nonlinear functions but fall short of robustness to model errors and external disturbances.

There are also some other control methods implemented on MWIP models. Lin *et al*. [6] adopted adaptive control for self-balancing and yaw motion control of two-wheeled mobile vehicle. The nested saturation control design technique was applied to derive a control law for a two-wheeled vehicle [7]. Adaptive robust dynamic balance and motion control are considered to handle the parametric and functional uncertainties [14]. Jung [15] presented a method for online learning and control of an MWIP by using neural networks.

The sliding mode control (SMC) approach might be an appropriate means to deal with uncertain MWIP systems because SMC is less sensitive to parameter variations and noise disturbances. It has been proven that an SMC algorithm can robustly stabilize a class of underactuated mechanical systems such as a mobile robot [16]. Park *et al*. [17] proposed an adaptive neural SMC method for trajectory tracking of nonholonomic wheeled mobile robots with model uncertainties and external disturbances. We proposed a velocity control method for the MWIP based on sliding mode and a novel sliding surface [18]. Ashrafiuon [19] proposed an SMC approach for underactuated multibody systems. Tsai [20] proposed an adaptive sliding mode controller to hierarchical tracking control tri-wheeled mobile robots. Terminal sliding mode control (TSMC) of finite time mechanism is such a variable structure control idea whose formation and development are based on the introduction of a nonlinear function into sliding hyperplane. Compared to a linear sliding mode surface, terminal sliding mode has no switching control term and the chattering can be effectively alleviated [21]. On the other hand, TSMC can improve the transient performance substantially. So far, TSMC has been used successfully in control applications [22]–[26]. Compared to the conventional SMC, TSMC provides faster finite-time convergence and higher control precision. Nonlinear terminal sliding mode surface functions such as $s = \dot{e} + e^{p\backslash q}$ [22] or cubic polynomials [26] can be applied.

While the MWIP system has been successfully applied in many fields, it still has much room for improvement. For

Manuscript received December 2, 2011; revised April 20, 2012; accepted July 26, 2012. Manuscript received in final form August 18, 2012. Date of publication October 5, 2012; date of current version August 12, 2013. This work was supported in part by the National Natural Science Foundation of China under Grant 60975058 and Grant 61075095, and by the State Key Laboratory of Robotics and System under Grant SKLRS-2010-MS-11. Recommended by Associate Editor Y. Chen.

J. Huang with the Department of Control Science and Engineering, Huazhong University of Science and Technology, Wuhan 430074, China, and also with the State Key Laboratory of Robotics and System (e-mail: huang_jan@mail.hust.edu.cn).

F. Ding is with the Department of Control Science and Engineering, Huazhong University of Science and Technology, Wuhan 430074, China (e-mail: dingfeng@smail.hust.edu.cn).

T. Fukuda is with the Department of Micro-Nano Systems Engineering, Nagoya University, Nagoya 464-8603, Japan (e-mail: fukuda@mein.nagoyau.ac.jp).

T. Matsuno is with the Graduate School of Natural Science and Technology, Okayama University, Okayama 700-8530, Japan (e-mail: matsuno@cc.okayama-u.ac.jp).

Color versions of one or more of the figures in this paper are available online at http://ieeexplore.ieee.org.

Digital Object Identifier 10.1109/TCST.2012.2214439

Fig. 1. Mechanism of a UW-Car.

instance, drivers can only stand on the Segway vehicles during driving, which is not comfortable for prolonged operation. Another deficiency of Segway is that the body will not be always upright during operation. To overcome these shortcomings, a new vehicle called UW-Car is introduced in this paper. This novel structure includes an MWIP base and a movable seat driven by a linear motor along the straight moving direction. The adjustable seat can guarantee that the vehicle body is always upright during driving, which is further discussed in the following sections. The mechanism of a UW-Car is as shown in Fig. 1.

It is well known that the brake system is one of the most important parts related to the safety of vehicles, the main purpose of which is to reduce the speed or stop motion, or keep a stationary vehicle at rest. During driving, in order to keep a proper distance between vehicles, precise control of the braking action is particularly important. Therefore, studying the braking of mobile robots based on the MWIP structure is of great significance both from the practical and theoretical points of view. Kidane [27] proposed a tilt brake algorithm for a narrow commuter vehicle, which was verified for different low-speed maneuvers.

In this paper, a Lagrangian approach is used to derive the dynamic model of a UW-Car. Based on the model, TSMC approaches are proposed to realize the velocity and braking control of a UW-Car.

The rest of this paper is organized as follows. The model formulation and equilibrium analysis are discussed in Section II. Velocity control and optimal braking analysis are discussed in Sections III and IV. Some results based on MATLAB simulation as well as experiments on a real UW-Car are given in Section V. Comparative studies between the MATLAB simulation results and those of the experiments are also performed. The effectiveness of the proposed methods is demonstrated through numerical simulation and experiments.

II. System Formulation

A. Dynamic Model

In this paper, a novel transportation system called UW-Car is investigated, which is different from normal

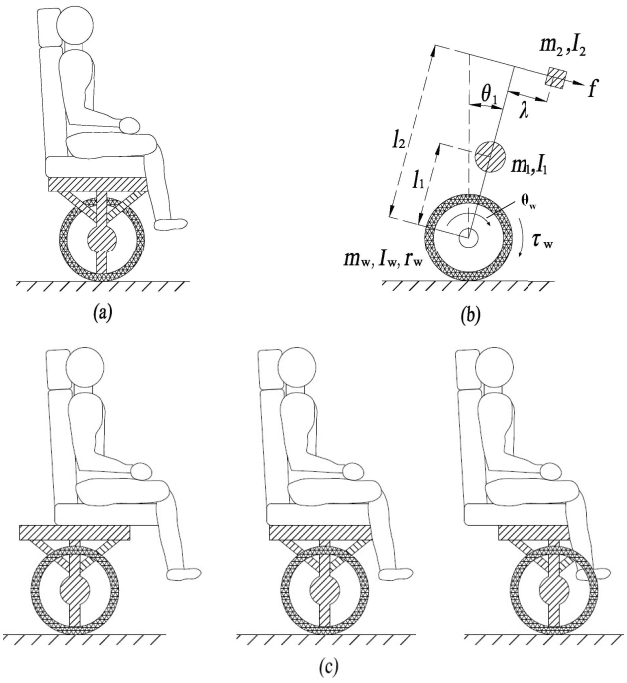

Fig. 2. (a) Prototype of a UW-car. (b) Model of a UW-car. (c) Movable seat of a UW-car at different positions.

MWIP systems. The UW-Car system is modeled as a 1-D inverse pendulum rotating along the wheels' axis with a movable seat above. The seat moves forward and backward on the top of the MWIP along the moving direction. The structure of the UW-Car system is described in Fig. 2, where θ_w and θ_1 are the wheel's rotation angle and the body inclination angle, respectively. λ denotes the displacement of the seat. We assume that the system moves on a flat ground. To simplify the model derivation, we divide the UW-Car system into three parts: the body, the seat, and the wheels. Some notations are introduced first:

m_1, m_2, m_w denote the masses of the body, the seat and the wheel;

I_b, I_s, I_w are the moments of inertia of the body, the seat, and the wheel;

l_1 is the distance between the wheel axle and the center of gravity of the body;

l_2 is the distance between the wheel axle and the plane of the movable seat;

r_w is the radius of the wheel;

D_1 is the viscous resistance in the driving system;

D_2 is the viscous resistance of the moving seat;

D_w is the viscous resistance of the ground;

τ_w is the torque of the motor driving wheels;

f is the force for the linear motor driving the seat.

It should be pointed out that only straight-line movement is considered here. Hence, a 3-D model [11] is not required. The following 3-D vector is used to describe the dynamic model of a UW-Car system: $\mathbf{q} = [\,\theta_w\ \theta_1\ \lambda\,]^T$.

To simplify the representation, we assume $S_1 = \sin\theta_1, C_1 = \cos\theta_1$. The coordinates of the wheels, the body, and the seat are denoted by$\mathbf{x_w} = [\,x_w\ y_w\,]^T$, $\mathbf{x}_1 = [\,x_1\ y_1\,]^T$, and $\mathbf{x}_2 = [\,x_2\ y_2\,]^T$, respectively.

The coordinate system of a UW-Car is depicted in Fig. 2(b). The positions and velocities of the three parts of a UW-Car system are given by

$$\begin{cases} x_w = r_w\theta_w \\ y_w = 0 \end{cases} \quad \begin{cases} \dot{x}_w = r_w\dot{\theta}_w \\ \dot{y}_w = 0 \end{cases} \tag{1}$$

$$\begin{cases} x_1 = r_w\theta_w + l_1S_1 \\ y_1 = l_1C_1 \end{cases} \quad \begin{cases} \dot{x}_1 = r_w\dot{\theta}_w + l_1C_1\dot{\theta}_1 \\ \dot{y}_1 = -l_1S_1\dot{\theta}_1 \end{cases} \tag{2}$$

$$\begin{cases} x_2 = r_w\theta_w + l_2S_1 \\ \quad +\lambda C_1 \\ y_2 = l_2C_1 - \lambda S_1 \end{cases} \quad \begin{cases} \dot{x}_2 = r_w\dot{\theta}_w + (l_2C_1 - \lambda S_1)\,\dot{\theta}_1 \\ \quad +\dot{\lambda}C_1 \\ \dot{y}_2 = -(l_2S_1 + \lambda C_1)\,\dot{\theta}_1 - \dot{\lambda}S_1. \end{cases} \tag{3}$$

Lagrange's equation of motion is used to analyze the dynamics of the system. The kinetic, potential, and dissipated energy are computed as follows.

Kinetic energy is represented by $T = T_w + T_1 + T_2$, where T_w, T_1, and T_2 are the kinetic energies of the wheels, the body, and the seat, respectively

$$T_w = \frac{1}{2}m_w\dot{\mathbf{x}}_\mathbf{w}^\mathbf{T}\dot{\mathbf{x}}_\mathbf{w} + \frac{1}{2}I_w\dot{\theta}_w^2 = \frac{1}{2}m_w r_w^2\dot{\theta}_w^2 \ + \frac{1}{2}I_w\dot{\theta}_w^2 \tag{4}$$

$$\begin{aligned} T_1 &= \frac{1}{2}m_1\dot{\mathbf{x}}_\mathbf{1}^\mathbf{T}\dot{\mathbf{x}}_\mathbf{1} + \frac{1}{2}I_b\dot{\theta}_1^2 \\ &= \frac{1}{2}m_1\left(r_w\dot{\theta}_w + l_1C_1\dot{\theta}_1\right)^2 + \frac{1}{2}m_1l_1^2S_1^2\dot{\theta}_1^2 + \frac{1}{2}I_b\dot{\theta}_1^2 \end{aligned} \tag{5}$$

$$\begin{aligned} T_2 &= \frac{1}{2}m_2\dot{\mathbf{x}}_\mathbf{2}^\mathbf{T}\dot{\mathbf{x}}_\mathbf{2} + \frac{1}{2}I_s\dot{\theta}_1^2 \\ &= \frac{1}{2}m_2\Big(\dot{\lambda}^2 + l_2^2\dot{\theta}_1^2 + \lambda^2\dot{\theta}_1^2 + r_w^2\dot{\theta}_w^2 + 2r_wC_1\dot{\theta}_w\dot{\lambda} \\ &\qquad +2r_w\left(l_2C_1 - \lambda S_1\right)\dot{\theta}_w\dot{\theta}_1 + 2l_2\dot{\theta}_1\dot{\lambda}\Big) + \frac{1}{2}I_s\dot{\theta}_1^2. \end{aligned} \tag{6}$$

The potential energy of the UW-Car system is written as

$$U = m_1gl_1C_1 + m_2g\left(l_2C_1 - \lambda S_1\right). \tag{7}$$

The energy is dissipated because of the friction between the wheels and ground in the driving system and the moving seat. The dissipated energy is

$$E_D = \frac{1}{2}D_w\dot{\theta}_w^2 + \frac{1}{2}D_1\dot{\theta}_1^2 + \frac{1}{2}D_2\dot{\lambda}^2. \tag{8}$$

The equations of motion are derived by the application of Lagrange's equation

$$\frac{d}{dt}\left(\frac{\partial T}{\partial\dot{\mathbf{q}}}\right) - \frac{\partial T}{\partial\mathbf{q}} + \frac{\partial U}{\partial\mathbf{q}} + \frac{\partial E_D}{\partial\dot{\mathbf{q}}} = \mathbf{B}\tau$$

where $\tau = [\tau_\mathrm{w}\ \mathrm{f}]^\mathrm{T}$.

Lagrange's equation leads to a second-order underactuated model with three variables and two inputs given by

$$\begin{aligned} &M_{11}\ddot{\theta}_w + (M_{12}C_1 - m_2r_w\lambda S_1)\,\ddot{\theta}_1 + m_2r_wC_1\ddot{\lambda} \\ &\quad = \tau_w - D_w\dot{\theta}_w + (M_{12}S_1 + m_2r_w\lambda C_1)\,\dot{\theta}_1^2 + 2m_2r_wS_1\dot{\theta}_1\dot{\lambda} \\ &(M_{12}C_1 - m_2r_w\lambda S_1)\,\ddot{\theta}_w + \left(M_{22} + m_2\lambda^2\right)\ddot{\theta}_1 + m_2l_2\ddot{\lambda} \\ &\quad = -\tau_w - D_1\dot{\theta}_1 + G_1S_1 + m_2g\lambda C_1 - 2m_2\lambda\dot{\theta}_1\dot{\lambda} \\ &m_2r_wC_1\ddot{\theta}_w + m_2l_2\ddot{\theta}_1 + m_2\ddot{\lambda} \\ &\quad = f - D_2\dot{\lambda} + m_2\lambda\dot{\theta}_1^2 + m_2gS_1 \end{aligned} \tag{9}$$

where M_{11}, M_{12}, M_{22}, and G_1 are given in Appendix.

The vector form of the Lagrange's equations for a UW-Car system is given by

$$\mathbf{M}\left(\mathbf{q}\right)\ddot{\mathbf{q}} + \mathbf{N}\left(\mathbf{q},\dot{\mathbf{q}}\right) = \mathbf{B}\tau \tag{10}$$

where the matrices $\mathbf{M}(\mathbf{q})$, $\mathbf{N}(\mathbf{q})$, and $\mathbf{B}$ are also given in the Appendix.

B. Analysis of Equilibriums in Set-Point Velocity Control

Note that in the velocity control, we usually do not care for the exact position of the UW-Car. Therefore, let us choose the state variables as $\mathbf{x} = [\,x_1\ x_2\ x_3\ x_4\ x_5\,]^\mathrm{T} = [\,\theta_1\ \lambda\ \dot{\theta}_w\ \dot{\theta}_1\ \dot{\lambda}\,]^\mathrm{T}$. The state model of the UW-Car system can be represented by

$$\begin{cases} \dot{x}_1 = x_4 \\ \dot{x}_2 = x_5 \\ M_{11}\dot{x}_3 + (M_{12}C_{x1} - m_2r_wx_2S_{x1})\,\dot{x}_4 \\ \quad +m_2r_wC_{x1}\dot{x}_5 = \tau_w - D_wx_3 \\ \quad +(M_{12}S_{x1} + m_2r_wx_2C_{x1})\,x_4^2 + 2m_2r_wS_{x1}x_4x_5 \\ (M_{12}C_{x1} - m_2r_wx_2S_{x1})\,\dot{x}_3 \\ \quad +\left(M_{22} + m_2x_2^2\right)\dot{x}_4 + m_2l_2\dot{x}_5 = -\tau_w \\ \quad -D_1x_4 + G_1S_{x1} + m_2gC_{x1}x_2 - 2m_2x_2x_4x_5 \\ m_2r_wC_{x1}\dot{x}_3 + m_2l_2\dot{x}_4 + m_2\dot{x}_5 \\ = f - D_2x_5 + m_2x_2x_4^2 + m_2gS_{x1} \end{cases} \tag{11}$$

where $S_{x1} = \sin x_1$ and $C_{x1} = \cos x_1$.

The vector form of the state model is given by

$$\mathbf{R}(\mathbf{x})\cdot\dot{\mathbf{x}} = \mathbf{H}(\mathbf{x}) + \mathbf{K}\tau \tag{12}$$

where

$$\mathbf{K} = \begin{bmatrix} 0 & 0 & 1 & -1 & 0 \\ 0 & 0 & 0 & 0 & 1 \end{bmatrix}^T.$$

The matrices $\mathbf{R}(\mathbf{x})$ and $\mathbf{H}(\mathbf{x})$ are given in the Appendix.

Assuming that state $\mathbf{x}^* = [\,x_1^*\ x_2^*\ x_3^*\ x_4^*\ x_5^*]^\mathrm{T}$ is the desired equilibrium of (9), the following equation can be obtained:

$$x_2^* = \frac{D_wx_3^* - (m_1l_1 + m_2l_2)\,g\sin\left(x_1^*\right)}{m_2g\cos\left(x_1^*\right)}. \tag{13}$$

In the case of a velocity control problem, the desired velocity $\dot{\theta}_w^* = x_3^*$ is always given in advance. We expect that at equilibrium $x_1^* = x_4^* = x_5^* = 0$. It means that the UW-Car moves at a constant velocity x_3^* without any body inclination while keeping the seat in a fixed position. Accordingly, x_2^* can be rewritten as

$$x_2^* = \frac{D_wx_3^*}{m_2g}. \tag{14}$$

Normally, x_2^* is small because the viscous parameter D_w is usually small.

III. Velocity Control of UW-Car Based on TSMC

To ensure the UW-Car system is driven steadily, a special sliding surface and a sliding mode controller design scheme are proposed in this section.

There are two basic requirements of our TSMC controllers.

1) Only the situation where the UW-Car is running on a flat ground is considered.
2) The body should be kept upright and the seat should vibrate as little as possible while the UW-Car system is running.

In the rest of this paper, " ˆ " denotes that the terms are evaluated on the basis of parameters of the nominal system moving on a flat ground without any uncertainties and disturbances.

Assuming that matrix $\mathbf{M}(\mathbf{q})$ is invertible, we start by rewriting the general model (10) as

$$\ddot{\mathbf{q}} = F(\dot{\mathbf{q}}, \mathbf{q}) + \mathbf{G}(\dot{\mathbf{q}}, \mathbf{q})\,\tau \tag{15}$$

where

$$\mathbf{F} = \begin{bmatrix} F_1 & F_2 & F_3 \end{bmatrix}^T$$
$$\mathbf{G} = \begin{bmatrix} G_{11} & G_{21} & G_{31} \\ G_{12} & G_{22} & G_{32} \end{bmatrix}^T.$$

Correspondingly, the nominal system is given by

$$\ddot{\mathbf{q}} = \hat{F}(\dot{\mathbf{q}}, \mathbf{q}) + \hat{\mathbf{G}}(\dot{\mathbf{q}}, \mathbf{q})\,\tau. \tag{16}$$

Considering the underactuated feature of the UW-Car system, we have to reduce the system order to obtain the controller.

Choosing a new state variable $\mathbf{q_1} = [\,\theta_1 \;\; \lambda\,]^T$, the following subsystem is then investigated in the TSMC controller design:

$$\ddot{\mathbf{q}}_1 = \mathbf{F_1}(\mathbf{q}, \dot{\mathbf{q}}) + \mathbf{G_1}(\mathbf{q}, \dot{\mathbf{q}})\,\tau \tag{17}$$

where

$$\mathbf{F_1} = \begin{bmatrix} F_2 \\ F_3 \end{bmatrix}$$
$$\mathbf{G_1} = \begin{bmatrix} G_{21} & G_{22} \\ G_{31} & G_{32} \end{bmatrix}.$$

Similarly, the nominal subsystem can be represented as

$$\ddot{\mathbf{q}}_1 = \hat{\mathbf{F}}_\mathbf{1}(\mathbf{q}, \dot{\mathbf{q}}) + \hat{\mathbf{G}}_\mathbf{1}(\mathbf{q}, \dot{\mathbf{q}})\,\tau. \tag{18}$$

It is assumed that the following equations are satisfied:

$$\left|\hat{F}_i - F_i\right| \le \tilde{F}_i, \qquad \tilde{\mathbf{F}} = \begin{bmatrix} \tilde{F}_2 & \tilde{F}_3 \end{bmatrix}^T, \qquad \mathbf{G}_1 = (\mathbf{I} + \Delta)\,\hat{\mathbf{G}}_1 \tag{19}$$

where F_i and $\hat{F}_i$ represent the ith element of matrices $\mathbf{F}$ and $\hat{\mathbf{F}}$ with $i = 2, 3$. G_{ij} and $\hat{G}_{ij}$ represent the (i, j)th element of matrices $\mathbf{G}$ and $\hat{\mathbf{G}}$ with $i = 2, 3$, $j = 1, 2$. $\mathbf{I}$ is a 2×2 identity matrix, and Δ is composed of Δ_{ij} satisfying the following inequality:

$$\left|\Delta_{ij}\right| \le D_{ij}, D_{ij} > 0, \text{ and } \|\mathbf{D}\| < 1.$$

According to the TSMC method proposed in [26], the sliding surface is defined as follows:

$$\mathbf{s}(t) = \dot{\mathbf{e}}(t) + \mathbf{C}\mathbf{e}(t) - \mathbf{w}(t) \tag{20}$$

where $\mathbf{e}(t) = \mathbf{x}(t) - \mathbf{x_d}(t)$, and $\mathbf{x_d}(t)$ is the reference value. $\mathbf{C} = \mathrm{diag}(c_1, c_2, \ldots, c_m)$, $c_i > 0$, $\mathbf{w}(t) = \dot{\mathbf{v}}(t) + \mathbf{C}\mathbf{v}(t)$.

The TSMC method is applied to the subsystem (17). The inclination angle θ_1^* is expected to be zero and the desired position of seat λ^* can be obtained from (14). Define the following sliding surfaces:

$$\begin{aligned} s_1(t) &= \dot{\theta}_1 + c_1\left(\theta_1(t) - \theta_1^*\right) - \dot{v}_1(t) - c_1 v_1(t) \\ s_2(t) &= \dot{\lambda} + c_2\left(\lambda(t) - \lambda^*\right) - \dot{v}_2(t) - c_2 v_2(t) \end{aligned} \tag{21}$$

where c_1 and c_2 are positive constants. The augmenting functions v_1 and v_2 are designed as a cubic polynomials that guarantee assumption 1 in [26] holds.

Proposition 1: Suppose that the model uncertainties of a UW-Car system (15) satisfies (19); then the sliding surfaces (21) will be achieved while the inclination angle θ_1 converges to zero and the position of seat will reach λ^* in finite time if the following control law is applied to the system:

$$\tau = \hat{\mathbf{G}}_1^{-1}\left[-\hat{\mathbf{F}}_\mathbf{1} - C\dot{\mathbf{e}} + \ddot{\mathbf{v}} + C\dot{\mathbf{v}} - \mathbf{k}\,\mathrm{sgn}(\mathbf{s})\right] \tag{22}$$

where

$$\begin{aligned} &\mathbf{C} = \mathrm{diag}(c_1\ c_2), \mathbf{e} = [\,e_1\ e_2\,]^T = [\,\theta_1 - \theta_1^*\ \ \lambda - \lambda^*\,]^T \\ &\mathbf{v} = \begin{bmatrix} v_1 & v_2 \end{bmatrix}^T, \mathrm{sgn}(\mathbf{s}) = \mathrm{diag}\left(\mathrm{sgn}(s_1)\ \ \mathrm{sgn}(s_2)\right) \\ &\mathbf{k} = (\mathbf{I} - \mathbf{D})^{-1}\left(\tilde{\mathbf{F}} + \mathbf{D}\left|-\hat{\mathbf{F}}_1 - \mathbf{C}\dot{\mathbf{e}} + \ddot{\mathbf{v}} + \mathbf{C}\dot{\mathbf{v}}\right| + \mathbf{\Gamma}\right) \\ &\Gamma = \begin{bmatrix} \boldsymbol{\gamma}_1 & \gamma_2 \end{bmatrix}, \quad \gamma_i > 0. \end{aligned}$$

Proof: The proof of convergence is proposed in [26, Ths. 2 and 3].

Note that, although the proposed TSMC controllers do not aim at controlling the velocity of UW-Car, the UW-Car will finally approach a constant speed when it is stabilized at an equilibrium $\mathbf{q}_1 = [\,0\ \lambda^*\,]^T$. This can be easily understood from (14).

Proposition 2: Suppose that the following condition is satisfied:

$$M_{11} + M_{12}C_1 - m_2 r_w \lambda S_1 > 0. \tag{23}$$

The proposed TSMC controller (22) guarantees that the angular velocity $\dot{\theta}_w$ can converge to $\dot{\theta}_w^*$ when the UW-Car system is running on a flat ground.

Proof: Obviously the sliding surface is achieved in this special case. Adding first two equations of (9), it follows that:

$$\begin{aligned} &(M_{11} + M_{12}C_1 - m_2 r_w \lambda S_1)\,\ddot{\theta}_w + (m_2 r_w C_1 + m_2 l_2)\,\ddot{\lambda} \\ &\quad + \left(M_{12}C_1 + M_{22} - m_2 r_w \lambda S_1 + m_2\lambda^2\right)\ddot{\theta}_1 \\ &= -D_w\dot{\theta}_w - D_1\dot{\theta}_1 + 2m_2 r_w S_1 \dot{\theta}_1 \dot{\lambda} \\ &\quad + (M_{12}S_1 + m_2 r_w \lambda C_1)\,\dot{\theta}_1^2 + G_1 S_1 \\ &\quad + m_2 g \lambda C_1 - 2m_2\lambda\dot{\theta}_1\dot{\lambda}. \end{aligned} \tag{24}$$

Note that (24) represents the internal dynamic model of a UW-Car, which has nothing to do with the control input τ_w and f. The state variables of the dynamic model are always on the sliding surface and satisfy the following equations:

$$\begin{aligned} \dot{\theta}_1(t) + c_1(\theta_1(t) - \theta_1^*) - \dot{v}_1(t) - c_1 v_1(t) &= 0 \\ \dot{\lambda} + c_2\left(\lambda(t) - \lambda^*\right) - \dot{v}_2(t) - c_2 v_2(t) &= 0. \end{aligned} \tag{25}$$

Given the known initial states $\theta_1(0)$, $\dot{\theta}_1(0)$, $\lambda(0)$, $\dot{\lambda}(0)$, and the sliding mode surface functions v_1 and v_2, $\theta_1(t)$, $\dot{\theta}_1(t)$, $\ddot{\theta}_1(t)$, $\lambda(t)$, $\dot{\lambda}(t)$, and $\ddot{\lambda}(t)$ are obtained directly from (25). Substituting these solutions in (24), it follows that:

$$Q(t)\ddot{\theta}_w + D_w\dot{\theta}_w = P(t) \tag{26}$$

where $P(t)$ and $Q(t)$ are known time-dependent functions and $Q(t)$ satisfies

$$Q(t) = M_{11} + M_{12}C_1 - m_2 r_w \lambda S_1.$$

Equation (26) is a first-order linear differential function with respect to the angular velocity $\dot{\theta}_w$. Since $D_w > 0$, the stability of (26) is only related to $Q(t)$. Because the condition (23) is satisfied, the solution of (26) is asymptotic stable. From (25), it follows that θ_1, $\dot{\theta}_1$, λ, and $\dot{\lambda}$ converge to equilibrium, which results in the convergence of $\dot{\theta}_w$ to the desired angle velocity $\dot{\theta}_w^*$.

IV. Optical Braking Controller Designed Using SMC

A UW-Car system moving smoothly with a constant velocity was investigated in Section III. A braking strategy aiming at obtaining the shortest braking distance is discussed in this section.

We assume that the UW-Car system has been stabilized at the equilibrium $\mathbf{q_1^0} = [0\ \lambda_0]^T$ with a corresponding steady velocity V_0 before braking. A switching TSMC control strategy is proposed to brake the UW-Car system within the shortest distance. Because of the inertia of the seat, the system cannot brake smoothly at once. We have to adjust the position of the seat to guarantee that the velocity ultimately decreases to zero. In short, the whole procedure is divided into the following two phases.

Phase 1: Decrease the speed of a UW-Car to zero as soon as possible.

Phase 2: Adjust the position of seat to stop the system.

The two phases are depicted in Figs. 3(a) and 4, respectively.

For braking, we designed three TSMC controllers: TSMC1, TSMC2, and TSMC3 according to the analysis of the braking procedure and (22).

In phase 1, we assume that the UW-Car system has been stabilized at equilibrium $\mathbf{q_1^0} = [0\ \lambda_0]^T$ with a constant velocity V_0 before braking. TSMC1 is applied to decrease the velocity to $V_1 (V_1 < V_0)$ at equilibrium $\mathbf{q}_1^{(1)} = [0\ -\lambda_1]^T$ at time $t = T_{f0}$, and to keep the position of seat until the velocity is reduced to zero at the end of the phase 1 when $t = T_{f1}$. The distance that the UW-Car moves forward is denoted by *FS*, which can be computed as the area depicted by Fig. 3(b)

$$FS = r_w \cdot \text{area}(A_1 + A_2). \tag{27}$$

In (27), we use $\text{area}(A_1 + A_2)$ to denote the total area of shaded space A_1 and A_2, which is described by

$$\begin{aligned}\text{area}(A_1 + A_2) &= \text{area}(A_1) + \text{area}(A_2) \\ &= \int_0^{T_{f0}} \dot{\theta}_w(t)dt + \int_{T_{f0}}^{T_{f1}} \dot{\theta}_w(t)dt.\end{aligned}$$

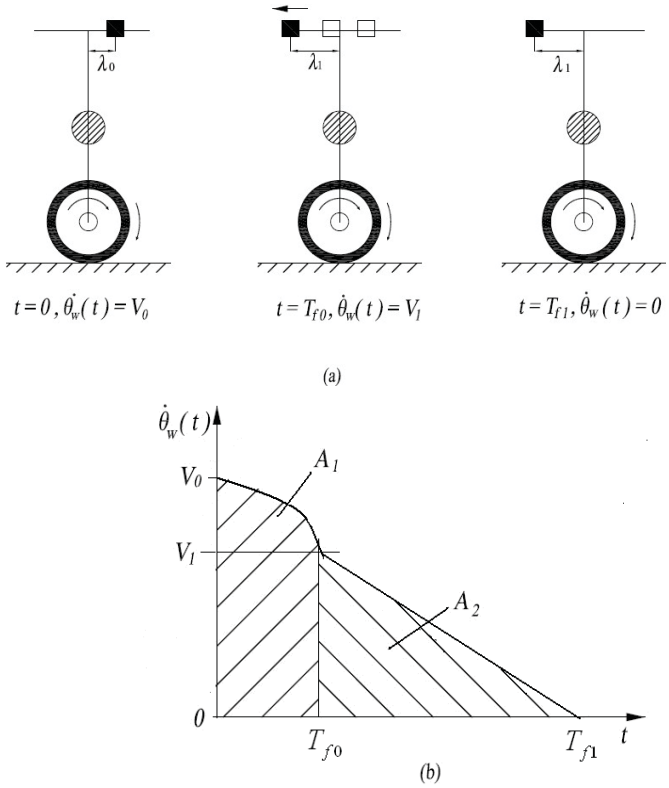

Fig. 3. (a) Procedure of the braking in phase 1. Decrease the speed to zero as soon as possible. (b) Braking distance of UW-car in phase 1.

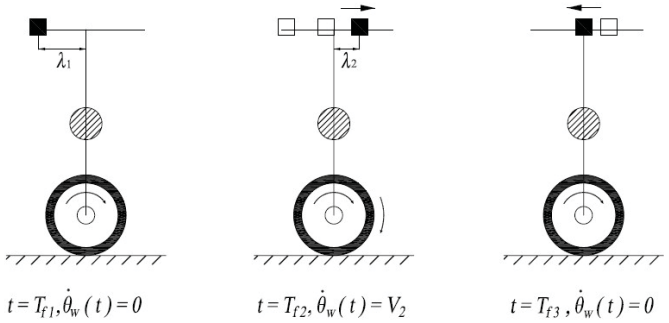

Fig. 4. Phase 2 of braking.

Note that $\text{area}(A_1 + A_2)$ represents the total angle of wheel rotation during the braking procedure. Therefore, *FS* describes the total braking distance.

In phase 2, at the beginning, the UW-Car stays at equilibrium $\mathbf{q}_1^{(1)} = [0\ -\lambda_1]^T$ with velocity $\dot{\theta}_w = 0$, which is the last state of phase 1. From time T_{f1}, the system will be controlled by TSMC2 until time T_{f2} and reaches equilibrium $\mathbf{q}_1^{(2)} = [0\ \lambda_2]^T$ with an appropriate instant velocity V_2, which guarantees that the system is finally stabilized at stable equilibrium $\mathbf{q}_1^{(3)} = [0\ 0]^T$. From time T_{f2} to time T_{f3}, the UW-Car system is controlled by TSMC3 and the system stops when time $t = T_{f3}$ at the equilibrium $\mathbf{q}_1^{(3)} = [0\ 0]^T$ finally.

The switching control diagram is shown in Fig. 5. The controllers are based on sliding surfaces given by

$$\begin{aligned}s_1(t) &= \dot{\theta}_1 + c_1\left(\theta_1(t) - \theta_1^*\right) - \dot{v}_1^{(i)}(t) - c_1 v_1^{(i)}(t) \\ s_2(t) &= \dot{\lambda} + c_2(\lambda(t) - \lambda_i) - \dot{v}_2^{(i)}(t) - c_2 v_2^{(i)}(t)\end{aligned} \tag{28}$$

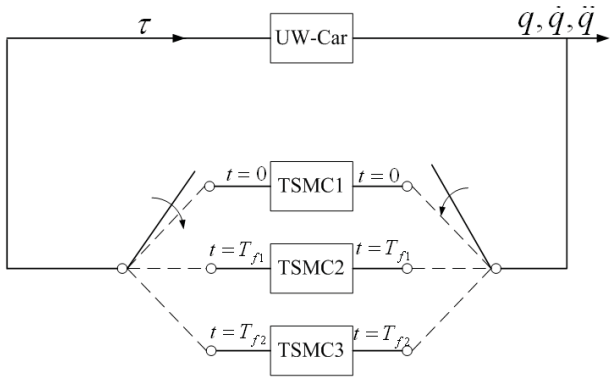

Fig. 5. Structure of switching TSMCs used for braking the UW-Car.

where

$$v_2^{(1)}(t)=\begin{cases} a_0^{(1)}+a_1^{(1)}t+a_2^{(1)}t^2+a_3^{(1)}t^3, & 0\le t\le T_{f0} \\ 0, & t>T_{f0}\end{cases} \quad (29)$$

$$v_2^{(2)}(t)=\begin{cases} a_0^{(2)}+a_1^{(2)}\left(t-T_{f1}\right)+a_2^{(2)}\left(t-T_{f1}\right)^2 \\ +a_3^{(2)}\left(t-T_{f1}\right)^3, & T_{f1}\le t\le T_{f2} \\ 0, & t>T_{f2}\end{cases} \quad (30)$$

$$v_2^{(3)}(t)=\begin{cases} a_0^{(3)}+a_1^{(3)}\left(t-T_{f2}\right)+a_2^{(3)}\left(t-T_{f2}\right)^2 \\ +a_3^{(3)}\left(t-T_{f2}\right)^3, & T_{f2}\le t\le T_{f3} \\ 0, & t>T_{f3}\end{cases} \quad (31)$$

$$a_0^{(i)}=\Delta_i,\quad a_1^{(i)}=0,\quad a_2^{(i)}=\frac{-3\Delta_i}{T_i^2},\quad a_3^{(i)}=\frac{2\Delta_i}{T_i^3}$$
$$\Delta_i=\lambda_{i-1}-\lambda_i,\qquad T_1=T_{f0},$$
$$T_{j+1}=T_{f(j+1)}-T_{fj}\qquad i=1,2,3,\qquad j=1,2 \quad (32)$$

Note that the initial and final positions of the seat are denoted by λ_0 and λ_3, respectively.

Proposition 3 (Calculation of Braking Distance): The distance through which the UW-Car moves forward in phase 1 is computed as

$$FS=r_w\cdot(\text{area}\,(A_1)+\text{area}\,(A_2)) \quad (33)$$

where

$$\begin{aligned}\text{area}(A_1)=&\frac{z_1^{(1)}}{24p}T_{f0}^4+\frac{1}{6}\left(\frac{z_2^{(1)}}{p}-\frac{z_1^{(1)}}{p^2}\right)T_{f0}^3\\&+\frac{1}{2}\left(\frac{z_3^{(1)}}{p}-\frac{z_2^{(1)}}{p^2}+\frac{z_1^{(1)}}{p^3}\right)T_{f0}^2\\&+\left(\frac{z_4^{(1)}}{p}-\frac{z_3^{(1)}}{p^2}+\frac{z_2^{(1)}}{p^3}-\frac{z_1^{(1)}}{p^4}\right)T_{f0}\\&+\frac{1}{p}\left(\frac{z_4^{(1)}}{p}-\frac{z_3^{(1)}}{p^2}+\frac{z_2^{(1)}}{p^3}-\frac{z_1^{(1)}}{p^4}-V_0\right)\\&\times\left(e^{-pT_{f0}}-1\right)\end{aligned}$$

$$\text{area}(A_2)=\frac{q_2\lambda_1}{p^2}\ln\left(1-\frac{pV_1}{q_2\lambda_1}\right)+\frac{V_1}{p}$$

$$\begin{aligned}V_1=\dot\theta_w\left(T_{f0}\right)=&\frac{z_1^{(1)}}{6p}T_{f0}^3+\frac{1}{2}\left(\frac{z_2^{(1)}}{p}-\frac{z_1^{(1)}}{p^2}\right)T_{f0}^2\\&+\left(\frac{z_3^{(1)}}{p}-\frac{z_2^{(1)}}{p^2}+\frac{z_1^{(1)}}{p^3}\right)T_{f0}\\&+\left(\frac{z_4^{(1)}}{p}-\frac{z_3^{(1)}}{p^2}+\frac{z_2^{(1)}}{p^3}-\frac{z_1^{(1)}}{p^4}\right)\\&-\left(\frac{z_4^{(1)}}{p}-\frac{z_3^{(1)}}{p^2}+\frac{z_2^{(1)}}{p^3}-\frac{z_1^{(1)}}{p^4}-V_0\right)e^{-pT_{f0}}\end{aligned}$$

$$p=\frac{D_w}{(m_w+m_1+m_2)r_w^2+I_w+m_1l_1r_w+m_2l_2r_w}$$
$$q_1=\frac{m_2(r_w+l_2)}{(m_w+m_1+m_2)r_w^2+I_w+m_1l_1r_w+m_2l_2r_w}$$
$$q_2=\frac{m_2g}{(m_w+m_1+m_2)r_w^2+I_w+m_1l_1r_w+m_2l_2r_w}$$
$$z_1^{(1)}=6c^2a_3^{(1)}q_1\quad z_2^{(1)}=2c^2a_2^{(1)}q_1\quad z_3^{(1)}=-6a_3^{(1)}q_1$$
$$z_4^{(1)}=\left(c^2\lambda_0-2a_2^{(1)}\right)q_1\qquad c=\sqrt{q_2/q_1}.$$

Proof: From time 0 to time T_{f0}, the system state $\mathbf{q_1}$ is always on the sliding surface of TSMC1. Thus the dynamics of the whole system can be represented by the following equations:

$$\begin{aligned}&\dot\lambda+c_2(\lambda-\lambda_1)-\dot v_2^{(1)}(t)-c_2v_2^{(1)}(t)=0\\&(M_{11}+M_{12})\ddot\theta_w+m_2(r_w+l_2)\ddot\lambda=-D_w\dot\theta_w+m_2g\lambda.\end{aligned} \quad (34)$$

The second equation of (34) is derived by substituting $\theta_1=0$, $\dot\theta_1=0$, and $\ddot\theta_1=0$ into the internal dynamics (24). Since the functions $v_2^{(1)}(t)$ and $\dot v_2^{(1)}(t)$ are known, it is apparent that $\lambda(t)$ can be easily solved from the first equation of (34). Substituting the solution of $\lambda(t)$ and its derivatives into the second equation, it is rewritten as a linear first-order differential equation with respect to the angular velocity $\dot\theta_w(t)$. With the initial conditions $\lambda(0)=\lambda_0$, $\dot\lambda(0)=0$, and $\dot\theta_w(0)=V_0$, $\dot\theta_w$ can also be solved as follows:

$$\begin{aligned}\dot\theta_w(t)=&\frac{z_1^{(1)}}{6p}t^3+\frac{1}{2}\left(\frac{z_2^{(1)}}{p}-\frac{z_1^{(1)}}{p^2}\right)t^2+\left(\frac{z_3^{(1)}}{p}-\frac{z_2^{(1)}}{p^2}+\frac{z_1^{(1)}}{p^3}\right)t\\&+\left(\frac{z_4^{(1)}}{p}-\frac{z_3^{(1)}}{p^2}+\frac{z_2^{(1)}}{p^3}-\frac{z_1^{(1)}}{p^4}\right)\\&-\left(\frac{z_4^{(1)}}{p}-\frac{z_3^{(1)}}{p^2}+\frac{z_2^{(1)}}{p^3}-\frac{z_1^{(1)}}{p^4}-V_0\right)e^{-pt}.\end{aligned} \quad (35)$$

Therefore, area(A_1) is computed as

$$\begin{aligned}\text{area}(A_1)=&\int_0^{T_{f0}}\dot\theta_w(t)dt=\frac{z_1^{(1)}}{24p}T_{f0}^4+\frac{1}{6}\left(\frac{z_2^{(1)}}{p}-\frac{z_1^{(1)}}{p^2}\right)T_{f0}^3\\&+\frac{1}{2}\left(\frac{z_3^{(1)}}{p}-\frac{z_2^{(1)}}{p^2}+\frac{z_1^{(1)}}{p^3}\right)T_{f0}^2\\&+\left(\frac{z_4^{(1)}}{p}-\frac{z_3^{(1)}}{p^2}+\frac{z_2^{(1)}}{p^3}-\frac{z_1^{(1)}}{p^4}\right)T_{f0}\\&+\frac{1}{p}\left(\frac{z_4^{(1)}}{p}-\frac{z_3^{(1)}}{p^2}+\frac{z_2^{(1)}}{p^3}-\frac{z_1^{(1)}}{p^4}-V_0\right)\\&\times\left(e^{-pT_{f0}}-1\right).\end{aligned} \quad (36)$$

From time T_{f0} to time T_{f1}, the dynamic of the UW-Car system can be represented by the following equations with initial velocity $\dot{\theta}_w(T_{f0}) = V_1$

$$\dot{\lambda} + c_2(\lambda - \lambda_1) = 0$$
$$(M_{11} + M_{12})\ddot{\theta}_w + m_2(r_w + l_2)\ddot{\lambda} = -D_w\dot{\theta}_w + m_2 g\lambda. \quad (37)$$

Similarly, area(A_2) is computed as

$$\text{area}(A_2) = \int_{T_{f0}}^{T_{f1}} \dot{\theta}_w(t)dt = \frac{q_2\lambda_1}{p^2}\ln\left(1 - \frac{pV_1}{q_2\lambda_1}\right) + \frac{V_1}{p}. \quad (38)$$

It is apparent that the area presented in Fig. 3(b) can be computed as area(A_1) + area(A_2). Therefore, (27) can be represented by (33).

Proposition 4: The velocity $\dot{\theta}_w(t)$ is reduced to V_2 at time $t = T_{f2}$, which guarantees that the velocity of the UW-Car system will become zero; meanwhile, the system state $\mathbf{q_1}$ converges to the equilibrium $q_1^{(3)} = [0\ 0]^T$ at the end of phase 2. Here, the constant velocity V_2 is chosen as

$$V_2 = \left[-\frac{z_1^{(2)}}{6p}T_3^3 - \frac{1}{2}\left(\frac{z_2^{(2)}}{p} - \frac{z_1^{(2)}}{p^2}\right)T_3^2 - \left(\frac{z_3^{(2)}}{p} - \frac{z_2^{(2)}}{p^2} + \frac{z_1^{(2)}}{p^3}\right)T_3 - \left(\frac{z_4^{(2)}}{p} - \frac{z_3^{(2)}}{p^2} + \frac{z_2^{(2)}}{p^3} - \frac{z_1^{(2)}}{p^4}\right)\right]e^{pT_3} - \left(\frac{z_4^{(2)}}{p} - \frac{z_3^{(2)}}{p^2} + \frac{z_2^{(2)}}{p^3} - \frac{z_1^{(2)}}{p^4}\right) \quad (39)$$

where

$$z_1^{(2)} = 6c^2a_3^{(3)}q_1 \quad z_2^{(2)} = 2c^2a_2^{(3)}q_1 \quad z_3^{(2)} = -6a_3^{(3)}q_1$$
$$z_4^{(2)} = \left(c^2\lambda_2 - 2a_2^{(3)}q_1\right).$$

Proof: Obviously only the nominal system (16) should be studied. TSMC2 ensures that the velocity of the UW-Car system can reach V_2 at time $t = T_{f2}$ while keeping the body inclination angle and the seat position at the equilibrium $\mathbf{q}_1^{(2)} = [0\ \lambda_2]^T$. From time T_{f2}, the system is controlled by TSMC3 with the sliding surface (31). The system state $\mathbf{q}_1$ is always on the sliding surface, and the dynamics of the system can be represented by the following equations when $T_{f2} \le t \le T_{f3}$:

$$\dot{\lambda} + c_2(\lambda - \lambda_3) - \dot{v}_2^{(3)}(t) - c_2v_2^{(3)}(t) = 0$$
$$(M_{11} + M_{12})\ddot{\theta}_w + m_2(r_w + l_2)\ddot{\lambda} = -D_w\dot{\theta}_w + m_2 g\lambda. \quad (40)$$

The final velocity can be computed by (40) with initial conditions $\dot{\lambda}(T_{f2}) = 0$, $\lambda(T_{f2}) = \lambda_2$, and $\dot{\theta}_w(T_{f2}) = V_2$. The solution of $\dot{\theta}_w(t)$ is obtained as follows:

$$\dot{\theta}_w(t) = \frac{z_1^{(2)}}{6p}(t - T_{f2})^3 + \frac{1}{2}\left(\frac{z_2^{(2)}}{p} - \frac{z_1^{(2)}}{p^2}\right)(t - T_{f2})^2 + \left(\frac{z_3^{(2)}}{p} - \frac{z_2^{(2)}}{p^2} + \frac{z_1^{(2)}}{p^3}\right)(t - T_{f2}) + \left(\frac{z_4^{(2)}}{p} - \frac{z_3^{(2)}}{p^2} + \frac{z_2^{(2)}}{p^3} - \frac{z_1^{(2)}}{p^4}\right) - \left(\frac{z_4^{(2)}}{p} - \frac{z_3^{(2)}}{p^2} + \frac{z_2^{(2)}}{p^3} - \frac{z_1^{(2)}}{p^4} - V_2\right)e^{-p(t-T_{f2})}. \quad (41)$$

TABLE I
PHYSICAL PARAMETERS OF THE UW-CAR SYSTEM

r_w	0.245	M	I_w	0.972	kg · m^2
m_w	32.4	kg	I_b	3.79	kg · m^2
m_1	137.6	kg	I_s	0.96	kg · m^2
m_2	8.7	kg	D_w	2.3	N · s/rad
l_1	0.166	M	D_1	0.1	N · s/rad
l_2	0.323	M	D_2	5.0	N · s/m

Substituting (39) in (41), we find that $\dot{\theta}(T_{f3})$ equals zero. Meanwhile, the system state $\lambda(t)$ converges to zero at time $t = T_{f3}$.

In order to obtain an optimal braking scheme, the braking distance *FS* has to be minimized. Thus, the following optimization problem should be solved:

$$\min_{\lambda_1, T_{f0}} (FS) \quad \text{s.t. } |\lambda_1| \le \lambda_{\max}, \quad T_{f0} > 0. \quad (42)$$

The genetic algorithm (GA), which is one of the most effective optimal research methods, is adopted to optimize parameters λ_1 and T_{f0}. The optimal λ_1^* and T_{f0}^* are regarded as the parameters of TSMC1.

As the main result of this section, the optimal braking scheme using the three TSMC controllers is illustrated as follows.

Step 1 (Optimization): Offline GA method is used to search for the optimal parameters (λ_1^* and T_{f0}^*) according to (42).

Step 2 (Braking): In phase 1, the optimal parameters computed by GA in Step 1 are chosen as the parameters of controller TSMC1. Apply the controller TSMC1 to the UW-Car system at t = 0 to ensure that the velocity reaches zero as soon as possible and the distance through which UW-Car is moving forward is a minimum.

Step 3 (Adjustment 2–1): Apply the controller TSMC2 to the UW-Car system at the beginning of phase 2 to reach to an appropriate initial velocity V_2.

Step 4 (Adjustment 2-2): At time $t = T_{f2}$, switch the controller TSMC2 to the controller TSMC3, and the UW-Car system brakes steadily finally at time $t = T_{f3}$.

V. SIMULATION AND EXPERIMENT

In order to verify the proposed methods, several simulation studies are performed in MATLAB while some experiments are carried out in a real UW-Car.

In all simulations and experiments, we use the physical parameters given in Table I. All control algorithms represented in Sections III and IV are realized both in MATLAB and the physical environments.

A. Set-Point Velocity Control Simulation

1) Velocity Control Simulation Comparisons Between Linear Quadratic Regulator (LQR) and TSMC: A commonly used stabilization technique is the LQR. The plant state is chosen

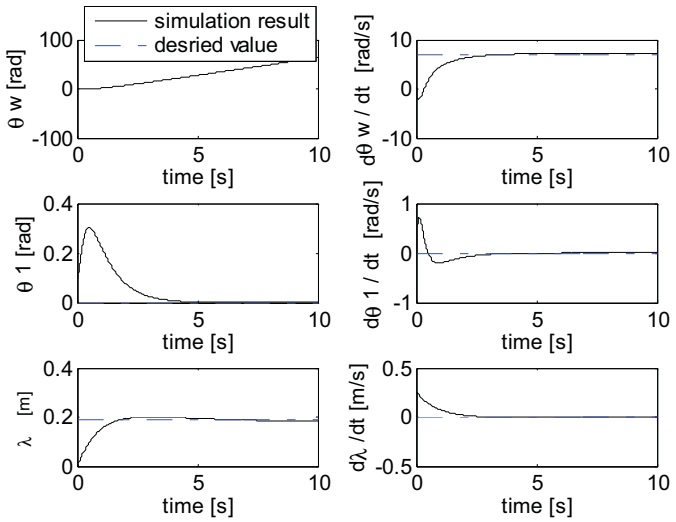

Fig. 6. Simulation results of a UW-Car system using LQR running at a constant velocity of 7 rad/s.

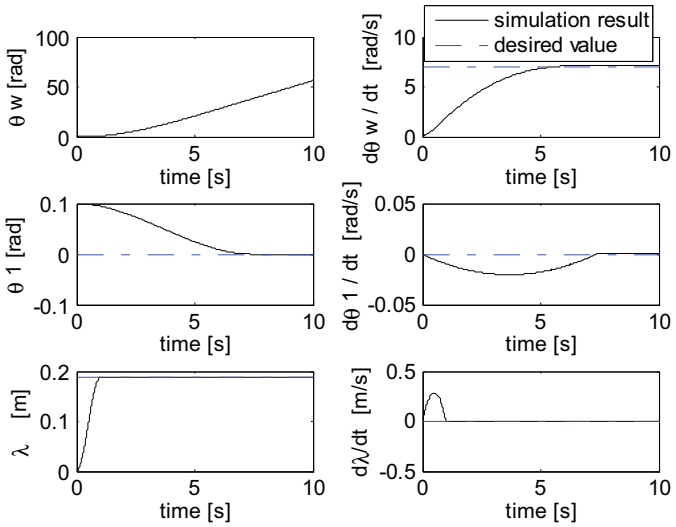

Fig. 7. Simulation results of a UW-Car system using TSMC running at a constant velocity of 7 rad/s.

as a 5-D vector given by $\mathbf{x} = [\theta_1\ \lambda\ \dot{\theta}_w\ \dot{\theta}_1\ \dot{\lambda}\ ]^T$. The desired equilibrium of the control system is $\mathbf{x}^* = [0\ \lambda^*\ \dot{\theta}_w^*\ 0\ 0]^T$. The LQR optimal control technique is used to design a linear state feedback control law $\tau = -\mathbf{K}\mathbf{x}$, where the gain matrix $\mathbf{K}$ minimizes the performance index

$$J = \int_0^\infty \left(\mathbf{x}^T\mathbf{Q}\mathbf{x} + \tau^T\mathbf{R}\tau\right)dt.$$

Weighted matrices $\mathbf{Q}$ and $\mathbf{R}$ were chosen as $\mathbf{Q} = \text{diag}(10\,000, 100, 100, 100, 10\,000)$, $\mathbf{R} = \text{diag}(0.01, 0.01)$. Assuming that the desired velocity satisfies $\dot{\theta}_w^* = 7$ rad/s and the desired distance of seat can be computed by (14), i.e., $\lambda^* = 0.1888$. The initial condition is chosen as $\lambda(0) = \dot{\lambda}(0) = 0$; $\theta_w(0) = \dot{\theta}_w(0) = \dot{\theta}_1(0) = 0$; and $\theta_1(0) = 0.1$. Solving the above linear quadratic problem, the gain matrix $\mathbf{K}$ is obtained

$$\mathbf{K} = \begin{bmatrix} -1.8665 & -0.5324 & -0.0839 & -0.7319 & -0.1586 \\ 0.0171 & 0.3167 & 0.0201 & 0.0248 & 0.9951 \end{bmatrix} \times 10^3.$$

The simulation results of the velocity control of a UW-Car running on the flat ground verify the ability of the designed LQR controller, and are shown by Fig. 6.

The dashed lines represent the desired value and the solid lines are the simulation trajectories. It turns out that the LQR controller has the ability to guarantee the inclination angle of the body to be approximately zero in finite time. However, the large overshoot and rapid change of states may make passengers feel uncomfortable.

To deal with the unknown perturbations and uncertainties of the UW-Car model, the TSMC method is investigated in the following due to its robustness to model uncertainties and external disturbances.

According to the analysis of Section III, a TSMC controller (22) is designed. The augmenting function $\mathbf{v}$ is designed as a cubic polynomial

$$v_i(t) = \begin{cases} a_{i0} + a_{i1}t + a_{i2}t^2 + a_{i3}t^3, & \text{if } 0 \le t \le T_i \\ 0, & \text{if } t > T_i \end{cases} \quad (43)$$

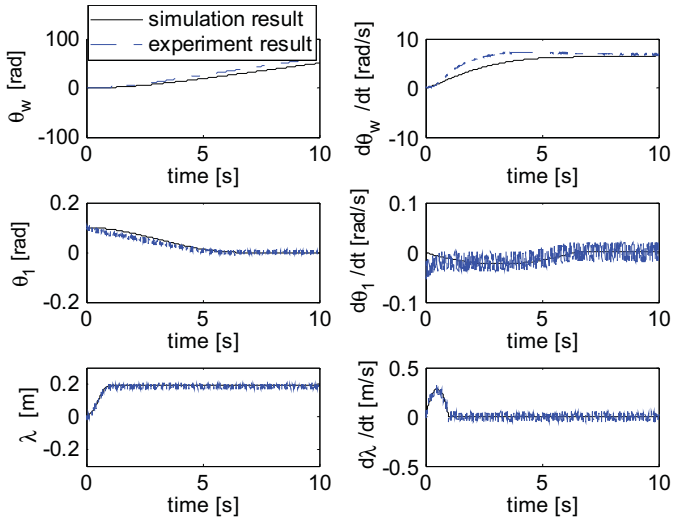

Fig. 8. TSMC velocity control comparison of MATLAB simulation and real experiment.

where

$$a_{i0} = e_i(0), \qquad a_{i1} = \dot{e}_i(0)$$
$$a_{i2} = -3\left(\frac{e_i(0)}{T_i^2}\right) - 2\left(\frac{\dot{e}_i(0)}{T_i^3}\right)$$
$$a_{i3} = 2\left(\frac{e_i(0)}{T_i^3}\right) + \left(\frac{\dot{e}_i(0)}{T_i^2}\right), \qquad i = 1, 2.$$

The TSMC controller parameters are chosen as $c_1 = 1$, $c_2 = 3.2$, $\gamma_1 = \gamma_2 = 10$, $\tilde{F} = 0.8\ F$, $D_1 = D_2 = 0.75$, and $T_1 = 6.4$ s, $T_2 = 1$ s with the same initial condition as in the LQR controller. The desired angle velocity is $\dot{\theta}_w^* = 7$ rad/s and the desired distance of the seat can be computed by (14), i.e., $\lambda^* = 0.1888$. In order to avoid the chattering associated with the SMC law, we have approximated the discontinuous sign function sgn(s) with a continuous saturation function of small boundary layers. The simulation results are shown in Fig. 7.

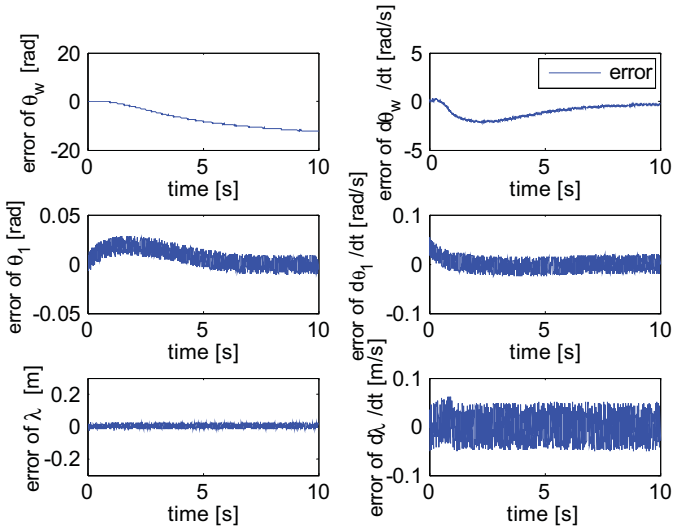

Fig. 9. Errors between MATLAB simulation and real experiment.

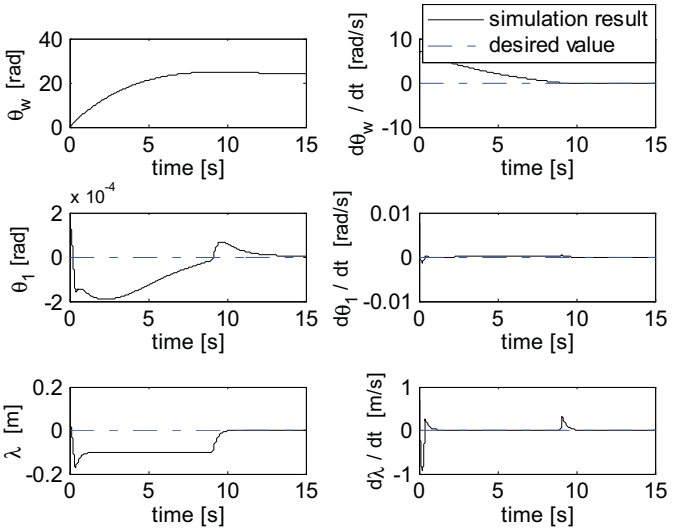

Fig. 11. Simulation results of braking a UW-Car system without optimal parameters.

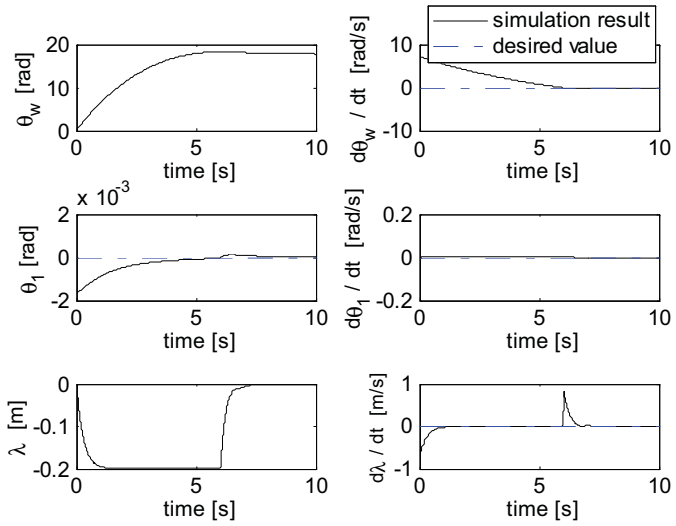

Fig. 10. Simulation results of braking a UW-Car system with optimal parameters.

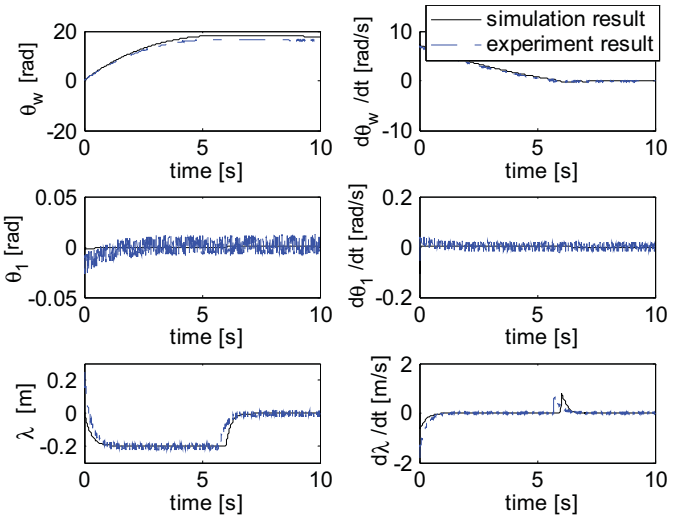

Fig. 12. Comparison of braking control using TSMC in MATLAB simulation and real experiment.

The dashed lines represent the desired value and the solid lines are the simulation trajectories. It turns out that the TSMC controller guarantees the inclination angle of the body to be approximately zero and the seat to vibrate only very slightly near a certain position. The TSMC controller takes a long time for the UW-Car system to accelerate to the desired velocity, but other performances such as overshoot and speed change are encouraging.

2) Velocity Control Comparisons Between Matlab Simulation and Experiment: Figs. 8 and 9 give the comparison results of the velocity control using TSMC. The dashed lines represent the experiment results and the solid lines are the MATLAB simulation results. It is obvious that the dashed lines follow the solid ones closely, and the differences are very small. In the real physical environment, there are small noises in the state trajectories.

B. Optimal Braking Control Simulation

1) Optimal Braking Control: We verify the effectiveness of optimal braking control by the simulation in MATLAB and real experiment.

The limit of seat displacement is $|\lambda_{\max}| = 0.2$. The constant λ_2 is chosen as $\lambda_2 = 0.05$. For the sliding surface given by (28)–(32), the controller parameters $c_1 = 1$, $c_2 = 3.57$, $T_2 = T_3 = 1$ s, and $D_1 = D_2 = 0.8$ were used. The optimal parameters are computed by GA as $\lambda^* = -0.2$, $T_{f0}^* = 0.01$. The initial condition is $\dot{\theta}_w = 7$ rad/s, $\theta_1 = \dot{\lambda} = \theta_w = \dot{\theta}_1 = 0$, $\lambda = 0.1888$; the simulation results are shown in Fig. 10. The UW-Car moving forward distance is about 4.41 m (18 $\times$ 0.245) and it takes about 5.8 s.

Fig. 11 shows the simulation results with parameters $\lambda_1 = -0.1$, $T_{f0} = 0.4$ and the same initial conditions in optimal braking control. The distance a UW-Car moving forward is about 6.40 m (26.11 $\times$ 0.245), and it takes

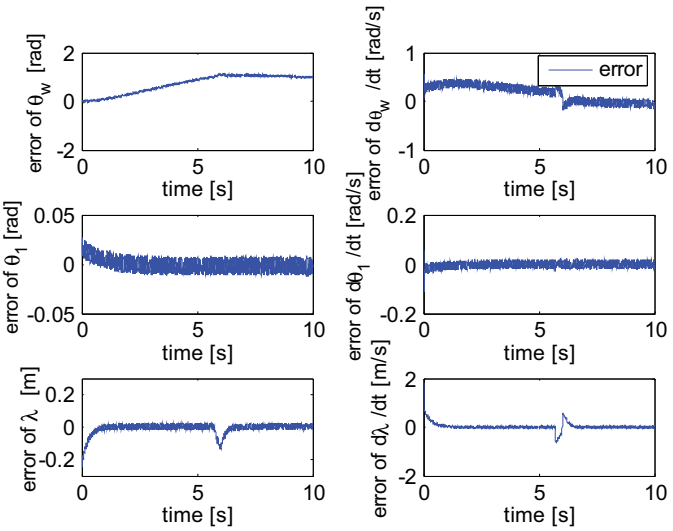

Fig. 13. Errors between MATLAB simulation and experiment.

approximately 9 s. Comparing the two sets of figures and data, we can conclude that the optimal braking control is effective.

2) Optimal Braking Control Comparisons Between Matlab Simulation and Experiment: Figs. 12 and 13 show the comparison results of the braking control. The dashed lines represent the experiment and the solid lines are the MATLAB simulation results. Because of the complexity of the braking algorithm, there are some differences between MATLAB simulation and the experiment. The accumulation of the velocity error results in the position error increasing at the beginning and converges to about 0.368 m (1.5×0.245) finally. Nevertheless, the simulations in MATLAB and experiment are consistent on the whole.

VI. Conclusion

A novel transportation system, called the UW-Car, which is composed of an MWIP base and a movable seat, was proposed in this paper. The dynamic model of the UW-Car system was obtained by applying Lagrange's equations of motion. Based on the model, velocity control and optimal braking strategy were discussed. A TSMC method was proposed for velocity control, which guaranteed that the UW-Car system could keep the body always upright and the seat in the desired position. Compared to the LQR method, the TSMC method presents better performance. A strategy of optimal braking with optimal parameters computed by GA algorithm was proposed, which guaranteed that the UW-Car system stopped in a short distance by implementing switching three terminal sliding mode controllers online. In order to prove the correctness of the model and the effectiveness of the algorithms, both simulations using MATLAB and experiments were performed. The comparison between MATLAB simulations and experiments confirmed the theoretical results.

Appendix

$$
\begin{aligned}
M_{11} &= (m_w + m_1 + m_2)\, r_w^2 + I_w \\
M_{22} &= m_1 l_1^2 + m_2 l_2^2 + I_b + I_s \\
M_{12} &= (m_1 l_1 + m_2 l_2)\, r_w \\
G_1 &= (m_1 l_1 + m_2 l_2)\, g \\
\mathbf{M(q)} &= \begin{bmatrix} M_{11} & M_{12}C_1 - m_2 r_w \lambda S_1 & m_2 r_w C_1 \\ M_{12}C_1 - m_2 r_w \lambda S_1 & M_{22} + m_2 \lambda^2 & m_2 l_2 \\ m_2 r_w C_1 & m_2 l_2 & m_2 \end{bmatrix} \\
\mathbf{N(q,\dot{q})} &= -\begin{bmatrix} -D_w \dot{\theta}_w + (M_{12}S_1 + m_2 r_w \lambda C_1)\,\dot{\theta}_1^2 + 2m_2 r_w S_1 \dot{\theta}_1 \dot{\lambda} \\ -D_1 \dot{\theta}_1 + G_1 S_1 + m_2 g \lambda C_1 - 2m_2 \lambda \dot{\theta}_1 \dot{\lambda} \\ -D_2 \dot{\lambda} + m_2 \lambda \dot{\theta}_1^2 + m_2 g S_1 \end{bmatrix} \\
\mathbf{B} &= \begin{bmatrix} 1 & -1 & 0 \\ 0 & 0 & 1 \end{bmatrix}^T \\
\mathbf{R(x)} &= \\
&\begin{bmatrix} 1 & 0 & 0 & 0 & 0 \\ 0 & 1 & 0 & 0 & 0 \\ 0 & 0 & M_{11} & M_{12}C_{x1} - m_2 r_w S_{x1} x_2 & m_2 r_w C_{x1} \\ 0 & 0 & M_{12}C_{x1} - m_2 r_w S_{x1} x_2 & M_{22} + m_2 x_2^2 & m_2 l_2 \\ 0 & 0 & m_2 r_w C_{x1} & m_2 l_2 & m_2 \end{bmatrix} \\
\mathbf{H(x)} &= \\
&\begin{bmatrix} x_4 \\ x_5 \\ -D_w x_3 + (M_{12}S_{x1} + m_2 r_w x_2 C_{x1})\, x_4^2 + 2m_2 r_w S_{1x} x_4 x_5 \\ -D_1 x_4 + G_1 S_{x1} + m_2 g x_2 C_{x1} - 2m_2 x_2 x_4 x_5 \\ -D_2 x_5 + m_2 x_2 x_4^2 + m_2 g S_{x1} \end{bmatrix}.
\end{aligned}
$$

References

[1] M. Sasaki, N. Yanagihara, O. Matsumoto, and K. Komoriya, "Steering control of the personal riding-type wheeled mobile platform," in *Proc. IEEE Int. Conf. Intell. Robot. Syst.*, Aug. 2005, pp. 1697–1702.

[2] D. P. Anderson. (2012). *nBot* [Online]. Available: http://www.geology.smu.edu/~dpa-www/robo/nbot/

[3] D. Kamen. (2010). Segway Company, San Francisco, CA [Online]. Available: http://www.segway.com/

[4] A. Salerno and J. Angeles, "A new family of two-wheeled mobile robots: Modeling and controllability," *IEEE Trans. Robot.*, vol. 23, no. 1, pp. 169–173, Feb. 2007.

[5] F. Grasser, A. D'Arrigo, S. Colombi, and A. Rufer, "Joe: A mobile, inverted pendulum," *IEEE Trans. Ind. Electron.*, vol. 49, no. 1, pp. 107–114, Feb. 2002.

[6] S. C. Lin, P. S. Tsai, and H. C. Huang, "Adaptive robust self-balancing and steering of a two-wheeled human transportation vehicle," *J. Intell. Robot. Syst. Theory Appl.*, vol. 62, no. 1, pp. 103–123, Apr. 2011.

[7] K. DucDo and G. Seet, "Motion control of a two-wheeled mobile vehicle with an inverted pendulum," *J. Intell. Robot. Syst.*, vol. 60, nos. 3–4, pp. 577–605, Dec. 2010.

[8] A. Salerno and J. Angeles, "The control of semi-autonomous two-wheeled robots undergoing large payload-variations," in *Proc. IEEE Int. Conf. Robot. Autom.*, Apr.–May 2004, pp. 1740–1745.

[9] Y.-S. Ha and S. Yuta, "Trajectory tracking control for navigation of the inverse pendulum type self-contained mobile robot," *Robot. Autonm. Syst.*, vol. 17, nos. 1–2, pp. 65–80, Apr. 1996.

[10] R. Marino, "On the largest feedback linearizable subsystem," *Syst. Control Lett.*, vol. 6, no. 5, pp. 345–351, Jan. 1986.

[11] K. Pathak, J. Franch, and S. K. Agrawal, "Velocity and position control of a wheeled inverted pendulum by partial feedback linearization," *IEEE Trans. Robot.*, vol. 21, no. 3, pp. 505–513, Jun. 2005.

[12] M. Karkoub and M. Parent, "Modeling and non-linear feedback stabilization of a two-wheel vehicle," *J. Syst. Control Eng.*, vol. 218, no. 8, pp. 675–686, Dec. 2004.

[13] M. W. Spong, "The swing up control problem for the Acrobat," *IEEE Control Syst. Mag.*, vol. 15, no. 1, pp. 49–55, Feb. 1995.

[14] Z. J. Li and J. Luo, "Adaptive robust dynamic valance and motion controls of mobile wheeled inverted pendulums," *IEEE Trans. Control Syst. Technol.*, vol. 17, no. 1, pp. 233–241, Jan. 2009.

[15] S. Jung and S. S. Kim, "Control experiment of a wheel-driven mobile inverted pendulum using neural network," *IEEE Trans. Control Syst. Technol.*, vol. 16, no. 2, pp. 297–303, Mar. 2008.
[16] V. Sankaranaryanan and A. D. Mahindrakar, "Control of a class of underactuated mechanical systems using sliding modes," *IEEE Trans. Robot.*, vol. 25, no. 2, pp. 459–467, Apr. 2009.
[17] B. S. Park, S. J. Yoo, J. B. Park, and Y. H. Choi, "Adaptive neural sliding mode control of nonholonomic wheeled mobile robots with model uncertainty," *IEEE Trans. Control Syst. Technol.*, vol. 17, no. 1, pp. 207–214, Jan. 2009.
[18] J. Huang, Z.-H. Guan, T. Matsuno, T. Fukuda, and K. Sekiyama, "Sliding-mode velocity control of mobile-wheeled inverted-pendulum systems," *IEEE Trans. Robot.*, vol. 26, no. 4, pp. 750–758, Aug. 2010.
[19] H. Ashrafiuon and R. S. Erwin, "Sliding control approach to underactuated multibody systems," in *Proc. Amer. Control Conf.*, 2004, pp. 1283–1288.
[20] P. S. Tsai, L. S. Wang, and F. R. Chang, "Modeling and hierarchical tracking control of tri-wheeled mobile robots," *IEEE Trans. Robot.*, vol. 22, no. 5, pp. 1055–1062, Oct. 2006.
[21] X. H. Yu and J. X. Xu, *Variable Structure Systems: Toward the 21st Century*. Berlin, Germany: Springer-Verlag, 2002.
[22] Z. H. Man, A. P. Paplinski, and H. R. Wu, "A robust MIMO terminal sliding mode control scheme for rigid robotic manipulators," *IEEE Trans. Autom. Control*, vol. 39, no. 12, pp. 2464–2469, Dec. 1994.
[23] S.-Y. Chen and F.-J. Lin, "Robust nonsingular terminal sliding model control for nonlinear magnetic bearing system," *IEEE Trans. Control Syst. Technol.*, vol. 19, no. 3, pp. 636–43, May 2011.
[24] H. Liu and J. F. Li, "Terminal sliding mode control for spacecraft formation flying," *IEEE Trans. Aerosp. Electron. Syst.*, vol. 45, no. 3, pp. 835–846, Jul. 2009.
[25] Y. S. Guo and C. Li, "Terminal sliding mode control for coordinated motion of a space rigid manipulator with external disturbance," *Appl. Math. Mech.*, vol. 29, no. 5, pp. 583–590, 2008.
[26] K.-B. Park and T. Tsuji, "Terminal sliding mode control of second-order nonlinear uncertain systems," *Int. J. Robust. Nonlinear Control*, vol. 9, no. 11, pp. 769–780, Sep. 1999.
[27] S. Kidane, R. Rajamani, L. Alexander, P. J. Starr, and M. Donath, "Development and experimental evaluation of a tilt stability control system for narrow commuter vehicles," *IEEE Trans. Control Syst. Technol.*, vol. 18, no. 6, pp. 1266–1279, Nov. 2010.

Jian Huang (M'07) received the B.Eng., M.Eng., and Ph.D. degrees in engineering from the Huazhong University of Science and Technology (HUST), Wuhan, China, in 1997, 2000, and 2005, respectively.

He was a Post-Doctoral Researcher with the Department of Micro-Nano Systems Engineering and Department of Mechano-Informatics and Systems, Nagoya University, Nagoya, Japan, from 2006 to 2008. He is currently an Associate Professor with the Department of Control Science and Engineering, HUST. His current research interests include rehabilitation robots, robotic assembly, networked control systems, and bioinformatics.

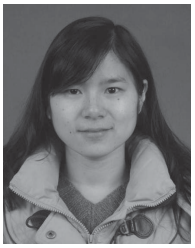

Feng Ding received the B.Eng. degree from the Chongqing University of Posts and Telecommunications, Chongqing, China, in 2008, and the Master of Engineering degree from the Huazhong University of Science and Technology, Wuhan, China, in 2012, where she is currently pursuing the Ph.D. degree, all in engineering.

Her current research interests include underactuated system control, system modeling, and applications of intelligent algorithms.

Toshio Fukuda (M'83–SM'93–F'95) received the B.S. degree from Waseda University, Tokyo, Japan, in 1971, and the M.S. and Dr.Eng. degrees from the University of Tokyo, Tokyo, in 1973 and 1977, respectively.

He was with the National Mechanical Engineering Laboratory, Tsukuba, Japan, from 1977 to 1982. From 1982 to 1989, he was with the Science University of Tokyo, Tokyo. Since 1989, he has been with Nagoya University, Nagoya, Japan, where he is currently a Professor with the Department of Micro-Nano Systems Engineering. His current research interests include intelligent robotic systems, cellular robotic systems, mechatronics, and micro- and nanorobotics.

Dr. Fukuda was the President of the IEEE Robotics and Automation Society from 1998 to 1999, the Director of the IEEE Division X, Systems and Control in 2001, and the Editor-in-Chief of the IEEE/ASME TRANSACTIONS ON MECHATRONICS from 2000 to 2002, and the President of the IEEE Nanotechnology Council from 2002 to 2005. He is the AdCom President of the IEEE Nanotechnology Council and the Director of the IEEE Region 10 from 2011 to 2012.

Takayuki Matsuno received the B.Eng., M.Eng., and Ph.D. degrees in engineering from Nagoya University, Nagoya, Japan, in 1998, 2000, 2005, respectively.

He joined the Department of Micro-Nano Systems Engineering and the Department of Mechano-Informatics and Systems, Nagoya University, as a Research Associate in March 2006. He was a Research Associate and Lecturer with the Intelligent Systems Design Engineering, Toyama Prefectural University, Toyama, Japan, in 2011. He is currently a Lecturer with the Graduate School of Natural Science and Technology, Okayama University, Okayama, Japan. His current research interests include flexible object manipulation, automation of assembly task in factories, and dynamical systems control.